2000

Convergence of Lateral Flow Along a Coastal Plain Estuary

Arnoldo Valle-Levinson
Old Dominion University

Chunyan Li
Old Dominion University

Kuo-Chuin Wong

Kamazima M. M. Lwiza

Original Publication Citation

Valle-Levinson, A., Li, C. Y., Wong, K. C., & Lwiza, K. M. M. (2000). Convergence of lateral flow along a coastal plain estuary. *Journal of Geophysical Research: Oceans, 105*(C7), 17045-17061. doi:10.1029/2000jc900025

JOURNAL OF GEOPHYSICAL RESEARCH, VOL. 105, NO. C7, PAGES 17,045-17,061, JULY 15, 2000

Convergence of lateral flow along a coastal plain estuary

Arnoldo Valle-Levinson and Chunyan Li

Center for Coastal Physical Oceanography, Department of Ocean, Earth, and Atmospheric Sciences
Old Dominion University, Norfolk, Virginia

Kuo-Chuin Wong

College of Marine Studies, University of Delaware, Newark

Kamazima M.M. Lwiza

Marine Sciences Research Center, State University of New York, Stony Brook

Abstract. A set of velocity profiles obtained in the James River estuary with an acoustic Doppler current profiler was used in combination with the results of an analytic tidal model to depict the appearance of surface lateral flow convergences ($\partial v / \partial y$) during both flood and ebb stages of the tidal cycle. The bathymetry of the estuary was characterized by a main channel and a secondary channel separated by relatively narrow shoals. Lateral surface flow convergences appeared over the edges of the channels and were produced by the phase lag of the flow in the channel relative to the shoals. Flood convergences developed in the late tidal stages and ebb convergences appeared soon after maximum currents. Most of these convergences caused fronts in the density field and flotsam lines that also appeared over the edges of the channel and that lasted <2 hours. The transverse flows associated with the convergences were mostly in the same direction throughout the water column. In fact, the vertically averaged flow produced the same convergence patterns as those near the surface. The analytic tidal model reproduced well the timing and location of the convergences as observed in the James River. Model results with different bathymetry emulated the results in other estuaries, e.g., axial convergence in an estuary with a channel in the middle. This work showed that the strength of lateral convergences along the estuary was proportional to the tidal amplitude and the channel steepness. It also suggested that the convergences were produced mainly by the tidal flow interacting with the channel-shoal bathymetry, i.e., that they did not require the presence of density gradients. However, the analytic model underestimated the magnitude of the convergences and did not account for vertical circulations associated with fronts. The formation of fronts resulted from the interaction of the tidal flow with the bathymetry and the density field.

1. Introduction

The study of convergences of lateral flow along an estuary has concentrated on the formation of axial fronts during flood tides only. *Brown et al.* [1991] presented widespread examples of convergence lines in several estuaries of the United Kingdom. *Nunes and Simpson* [1985] explained the formation of axial convergence fronts that developed in the middle of a channel in the Conwy, a vertically homogeneous estuary in north Wales. These features originated from the apex of a tidal intrusion front and were supposedly maintained by a surface transverse circulation from either bank of the estuary during flood. *Sarabun* [1980], *Simpson and Turrell* [1986], *Huzzey and Brubaker* [1988], *Turrell et al.* [1996], and *Swift et al.* [1996] used the argument of differential advection of the along-estuary density field by the laterally sheared along-estuary flow to explain their observations of axial convergence during late flood-early ebb stages. The observations of *Sarabun* [1980], *Huzzey and Brubaker* [1988], and *Swift et al.* [1996] actually showed the surface flow convergence over the edge, not in the middle of the channel. The presence of convergences over the channel edges is ubiquitous in other estuarine systems like the lower Chesapeake Bay [e.g., *Sletten et al.*, 1999] and in Mexican coastal lagoons with weak density gradients [*A. Valle-Levinson*, unpublished data, 1999]. In the present study, we document the development of surface convergences over the channel edges during both stages of the tidal cycle and propose the mechanism that favors the formation of convergences in the middle of the channel or over the edge of the channel.

Most of the above studies suggested that density gradients are crucial for the development of transverse circulation associated with axial convergences. In fact, *Swift et al.* [1996] postulated that transverse circulation is driven mainly by cross-channel density gradients. *Sarabun* [1980] and

Paper number 2000JC900025.
0148-0227/00/2000JC900025$09.00

Turrell et al. [1996], as well as *Valle-Levinson and O'Donnell* [1996], hypothesized that transverse circulation was a result of the interaction among the channel geometry (or bathymetry), the transverse shear of along-estuary flow, and the along-estuary density gradient. These are reasonable explanations for convergences that appear during late flood stages but cannot be used to explain along-estuary convergences during ebb stages. *Sarabun* [1980] and *Ferrier and Anderson* [1997] have pointed out the presence of fronts during ebb stages in the Delaware Bay and Tay estuaries, respectively, but did not support their observations with velocity measurements of sufficient lateral resolution. In this study, we propose that convergences of lateral flow along the estuary may develop during both ebb and flood stages even under homogeneous conditions. In other words, we propose that estuarine density gradients, contrary to existing theories, may have a small influence on the formation of along-estuary convergences. In this paper, the terms "convergence" and "divergence" are used in a right-handed coordinate system to denote one-dimensional lateral convergence or divergence (e.g., $\partial v/\partial y$, where v and y are the across-estuary flow and direction, respectively). This use is justified later from the fact that $\partial u/\partial x$ (where u and x are the along-estuary flow and direction, respectively) is relatively small compared to $\partial v/\partial y$.

The objectives of this study were to (1) document the development of convergences of lateral flow along the estuary during both stages of the tidal cycle and (2) explain their development over the edges of the channel or in the middle of the channel. Their development and location were documented with a set of velocity profiles measured across two sections of the James River in October (spring tides) and November (neap tides) 1996. The location and timing of the convergences were explained with an analytic tidal model that allowed arbitrary cross-channel bathymetry. In section 2, observations that show the presence of surface convergences over the edge of an estuarine channel during both ebb and flood stages are presented. This is followed by the presentation of the analytic model with results for different lateral distributions of bathymetry, including that of the James River sector studied. We then discuss the mechanism proposed for the formation of convergences, and we conclude with the main findings of this study.

2. Observation of Convergences

2.1. Data Collection and Processing

The data collection consisted of repeating cross-estuary transects as often as possible to capture the intratidal variability of the distribution of the flow and density fields across the lower James River estuary (Figure 1). Two transects, ~4 km long and separated by 1 km, were traversed in <1.5 hours. The dimensions of this sampling rectangle (~4 km by 1 km) allowed enough repetitions of the perimeter (at least eight) during one tidal cycle. This assured good quality and repeatability of the time series used for the data analysis and permitted the determination of the along-estuary consistency of the cross-estuary structure within each rectangle, i.e., at least within a distance of 1 km.

The two cross-estuary transects in the lower James River (Figure 1) were sampled throughout two spring (October 26-27) and two neap (November 2-3) semidiurnal tidal cycles in the fall of 1996. Each 25 hour long sampling effort consisted of continuous velocity and surface density (only during spring tides) measurements. Velocity data were obtained with a 600 kHz Broad Band RD Instruments acoustic Doppler current profiler (ADCP). Surface density values were recorded with a Sea Bird SBE-1621 thermosalinograph. One small boat (<10 m long) with the ADCP and thermosalinograph covered the two transects. The ADCP was mounted looking downward on a small (roughly 1.2 m long) catamaran and towed to the side of the boat at speeds of ~2.5 m s^{-1}. It recorded velocity profiles averaged over 30 s, which gave a horizontal spatial resolution of ~75 m. The bin size for vertical resolution was 0.5 m, and the closest bin to the surface was located at nearly 2 m. These settings gave a precision of 0.01 m/s and an accuracy of ~0.01 m s^{-1} for the measured velocities. Compass calibration and data correction were performed following *Joyce* [1989]. Navigation was carried out with differential Global Positioning System (GPS). The thermosalinograph recorded one value every 10 s; that is, it provided a spatial resolution of ~25 m. Time series of velocity profiles and of surface temperature and salinity recorded at each point along each transect consisted of 20 values for the spring tides cruise and 17 values for the neap tides cruise.

The bathymetry of the transects sampled consisted of two asymmetric channels separated by relatively narrow shoals. One of the channels (the northeastern or main channel) was roughly 3 times deeper than the other (the southwestern or secondary channel). The main channel was ~14 m deep in transect 1 and 11 m deep in transect 2, while the secondary channel was ~5 m deep in transect 1 and 4 m deep in transect 2. As will be seen, this bathymetric distribution played a key role in determining the position of convergences.

2.2. Description of Surface Convergences

In order to identify surface convergences in the tidal flow, the near-surface (2.2 m deep) velocity vectors were plotted as a function of time and distance from the northeastern point of each transect. These vectors were rotated to the direction of maximum variability of the tidal currents and were represented for spring tides and for neap tides (Figure 2). The vectors illustrated the magnitude of the surface flows observed, the periods of flood and ebb currents, and the times at which observations were made. Spring currents reached values of 1 m s^{-1} during ebb stages, while neap maximum currents were ~0.8 m s^{-1}. Inferences relative to regions of strong lateral shears in the along-estuary tidal flow u and convergences of the lateral flow v could be drawn from Figures 2a and 2b. For instance, late flood convergences appeared at transect 2 between 3.3 and 3.5 km (13 to 15 and 23 to 25 hours in Figure 2a) and at transect 1 between 2.6 and 2.9 km (same times, Figure 2b). Also, ebb convergences were identified near 2 km at transect 1 (19 to 21 and 30 to 32 hours in Figure 2b) and between 2.5 and 2.8 km at transect 2 (same times, Figure 2a). Nonetheless, owing to the fact that these representations were not synoptic the flows were interpolated to a uniform time versus distance grid. Interpolation was carried out through the construction of Delaunay triangulations with the Interactive Data Language (IDL) software. The gridded flows allowed the calculation of across-estuary convergences ($\partial v/\partial y$) as presented next for spring and neap tides separately.

2.2.1. Spring tides. The near-surface flow during spring tides exhibited convergences that persisted through flood and ebb over certain locations but that were phase locked over other locations (Plate 1). Over the secondary channel of

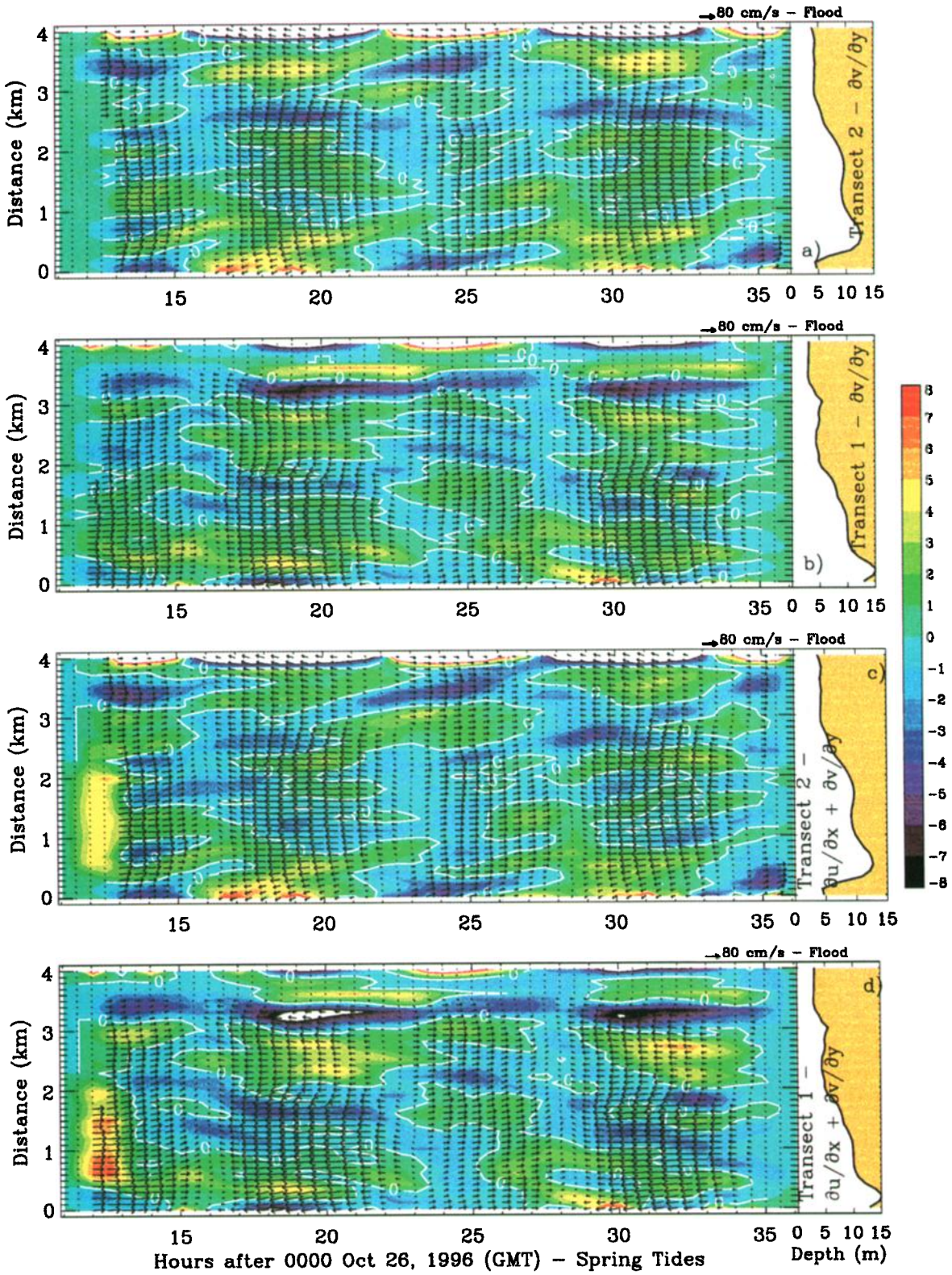

Plate 1. Surface velocity vectors interpolated to a uniform time-space grid during spring tides and the bathymetry associated with each transect. (a and b) Divergences obtained from $\partial v/\partial y$ only and (c and d) $\partial u/\partial x + \partial v/\partial y$ with the same color scale as Plates 1a and 1b. The colored contours denote values of divergence (10^{-4} s^{-1}) at intervals of 1 as shown by the scale on the right. Blue denotes convergences. The white contours separate positive (divergence) from negative (convergence) values. Flood flow points to the right.

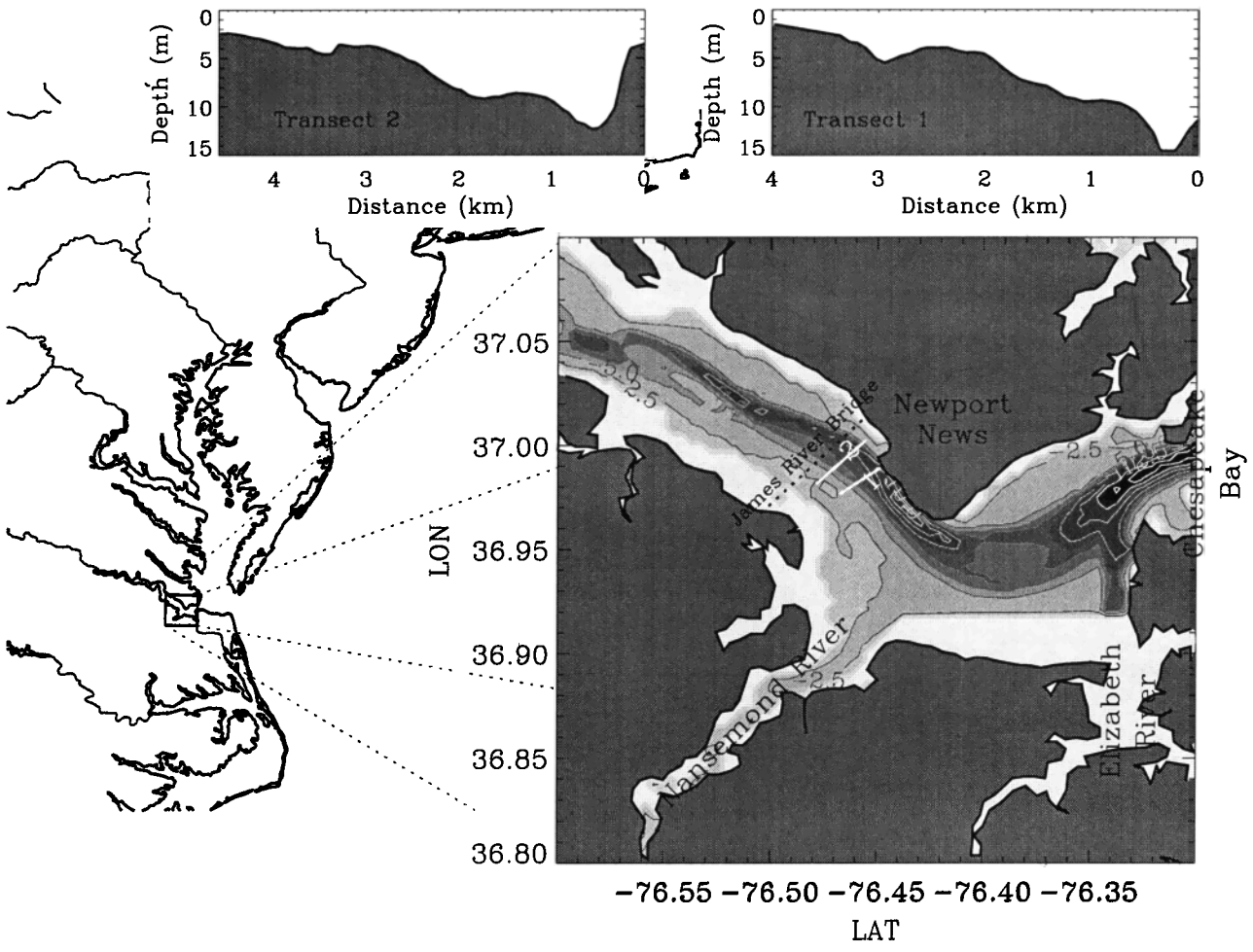

Figure 1. Map of the study area in the Chesapeake Bay showing the two transects where observations took place in the James River estuary. The transects are denoted by two solid white lines southeastward of the James River bridge (dotted line spanning both shores). The bathymetry of the area is shown in shaded contours at intervals of 2.5 m. In particular, the bathymetry of transects 1 and 2 is shown as separate plots.

transect 1, between 3 and 3.4 km in Plate 1b, convergences persisted throughout the tidal cycle. The flood flow converged at maximum rates of 2×10^{-4} s^{-1} over the shoal and at maximum rates of 8×10^{-4} s^{-1} over the channel edge during ebb. At the equivalent location in transect 2, between 3.3 and 3.8 km (Plate 1a), convergences only developed during flood periods (13 to 15 and 23 to 25 hours). Therefore the convergences over this region were coherent along the estuary only during flood stages. Over the southern (or left looking into the estuary) edge of the main channel, around 2 km in transect 1 (Plate 1b), a surface convergence was observed soon after maximum ebb (18.5 to 20 hours). Over the equivalent location in transect 2, between 2.5 and 2.8 km (Plate 1a), convergences of 5×10^{-4} s^{-1} also developed after maximum ebb (18.5 to 20 hours). A third region of convergence at both transects appeared over the northern (right looking into the estuary) edge of the main channel, near the northern end of each transect, between 0 and 0.2 km (13 to 15 and 23 to 25 hours).

The divergences determined with $\partial v/\partial y$ were qualitatively the same as those calculated with the total horizontal divergence $\partial v/\partial y + \partial u/\partial x$ (Plate 1). The contribution to the horizontal divergence by the along-estuary flow ($\partial u/\partial x$) could not be estimated with the same spatial resolution in x as for $\partial v/\partial y$ in y, but it was calculated from the two transects sampled 1 km apart. The magnitude of the divergences increased slightly with the inclusion of $\partial u/\partial x$ (Plates 1c and 1d for which the $\partial u/\partial x$ used is the same); however, the contours showed very similar patterns to those of $\partial v/\partial y$ (Plates 1a and 1b). This resemblance indicated that the contribution of $\partial u/\partial x$ was rather weak; in fact, it was typically 1 order of magnitude smaller than $\partial v/\partial y$. These patterns also implied that the horizontal divergence was appropriately represented with $\partial v/\partial y$ alone.

The locations that showed convergences at both transects 1 and 2 (Plate 1) have coherent along-estuary bathymetry between the transects. Therefore the along-estuary scale of these convergences appeared to be determined by the coherence scale of the bathymetry. This is because along-estuary changes of bathymetry would tend to alter the flow and convergence patterns as indicated by observations of the extent of the foam lines and by the analytic results presented later. In the analytic results the bathymetry is coherent along the estuary, and the convergences appeared all along the estuary. This is further addressed in section 4. Convergences observed during flood periods over the northern edge of the main channel were stronger in transect 2 than in transect 1 because there was no shoal at the northern end of transect 1, which ends at the Newport News Shipyard and limits the development of cross-channel flow from the flanks.

From the flow and convergence distributions presented in Plate 1, it could be proposed that front formation should be expected in two locations during end of flood and one location after maximum ebb owing to the along-estuary coherence of the convergence patterns in those locations. The two end-of-flood locations would be near the secondary channel and over the northern edge of the main channel, and the ebb location would be over the southern (left looking into the estuary) edge of the main channel.

In fact, the front development over the southern edge of the main channel was observed in the surface salinity field after maximum ebb (Plates 2a and 2b). This front was manifested by a change of isohaline orientation from perpendicular to the shores to parallel to the shores. The change of orientation was more pronounced in transect 1 than in transect 2; it lasted <2 hours and appeared at ~2 km between 18.5 and 20 hours and between 30.5 and 32 hours (Plate 2b). The end-of-flood convergence over the northern (right

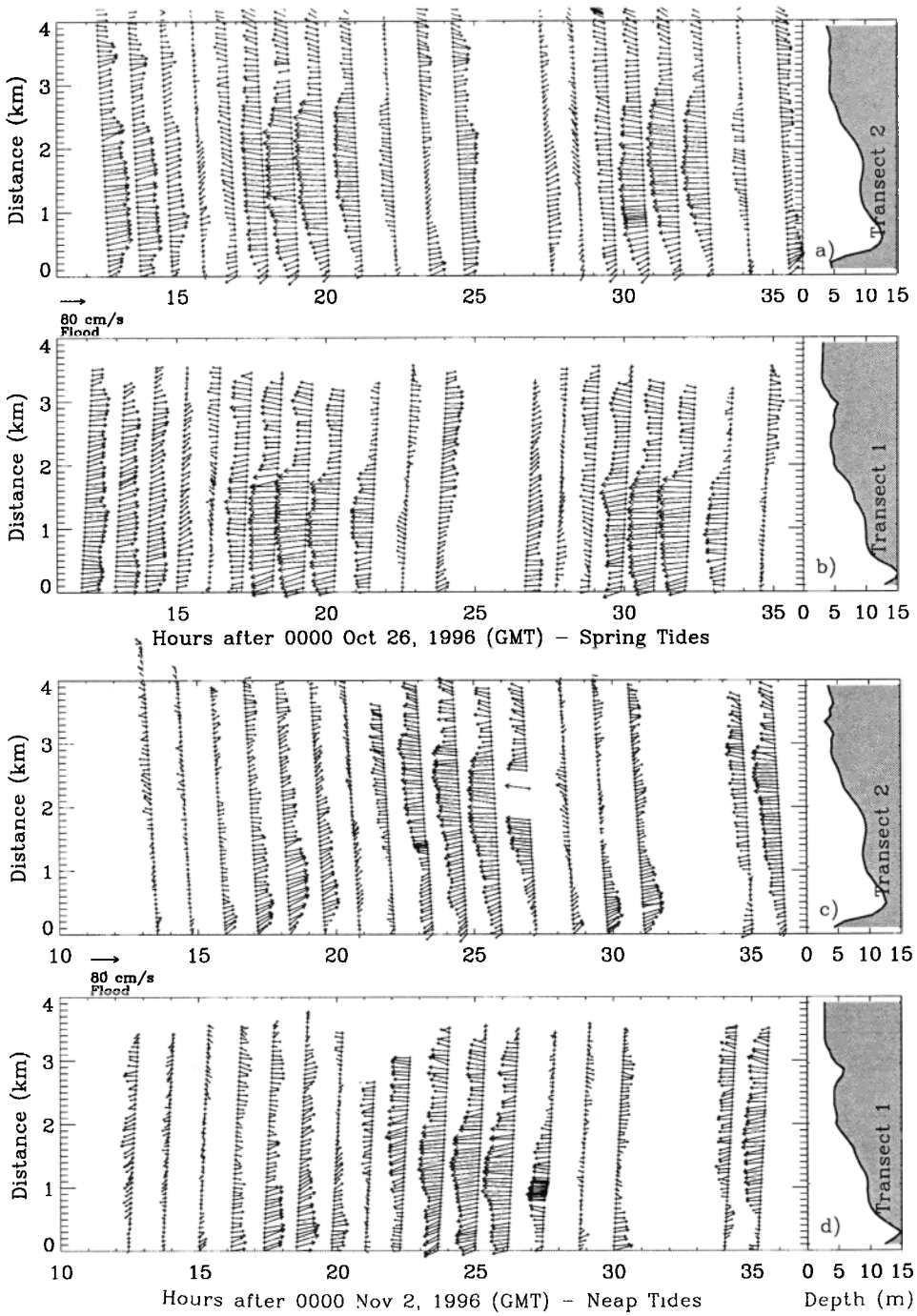

Figure 2. Instantaneous surface velocities across the estuary at the times of observation during (a and b) spring tides (October 26-27, 1996) and (c and d) neap tides (November 2-3, 1996). The bathymetry associated with each transect is shown on the right plots, with the depth scale appearing on the abscissa. Transect 2 was longer than transect 1, which is why the vectors are drawn beyond 4 km. Flood flow points to the right, as shown on the scale between Figures 2a and 2b and 2c and 2d.

looking into the estuary) edge of the main channel also reflected enhanced lateral gradients in salinity close to the origin (0 km) between 13.5 and 15 hours, and between 25.5 and 27 hours (Plate 2b). These ebb and flood fronts were also evident as flotsam lines observed on the surface at those times. The observed flood convergence over the secondary channel did not cause an apparent front in the salinity field. This suggested that convergences do not necessarily cause enhanced gradients in the density field and that regions of convergence are not necessarily produced by the density field; that is, convergences may occasionally exist in regions of weak density gradients.

The abrupt change in coastline orientation around Newport News, ~10 km to the south of the study area (Figure 1), may produce centrifugal accelerations that could influence the dynamics in the vicinity of the headland [e.g., *Geyer*, 1993; *Chant and Wilson*, 1997]. These curvature effects would induce secondary flows consisting of near-surface normal flows away from and near-bottom normal flows toward the headland. The study area must be far away enough from the direct influence of the headland because such secondary circulation pattern was not observed on the tidal flow. Cross sections of the velocity field associated with the convergences showed that the transverse flows associated with flood and ebb convergences were practically in the same direction throughout the water column (Figure 3). Similar patterns were observed by *Swift et al.* [1996] in the Piscataqua River, New Hampshire. In fact, the convergence/divergence patterns of Plate 1 were consistent with those estimated with the vertically averaged transverse flows ($\partial\bar{v}/\partial y$). The timing and location of the convergences were the same, but the rates of convergence were weaker, as expected from weaker vertical averages, than surface values. The near-surface convergence during ebb (Figures 3a and 3b) was actually associated with the southern edge of the outflow core; that is, it was found over the edge of the channel. The same could be said about the flood near-surface convergences over the southern (or left) edge of the channel (Figures 3c and 3d). In addition, flood convergences developed over the northern edge of the inflow core. The

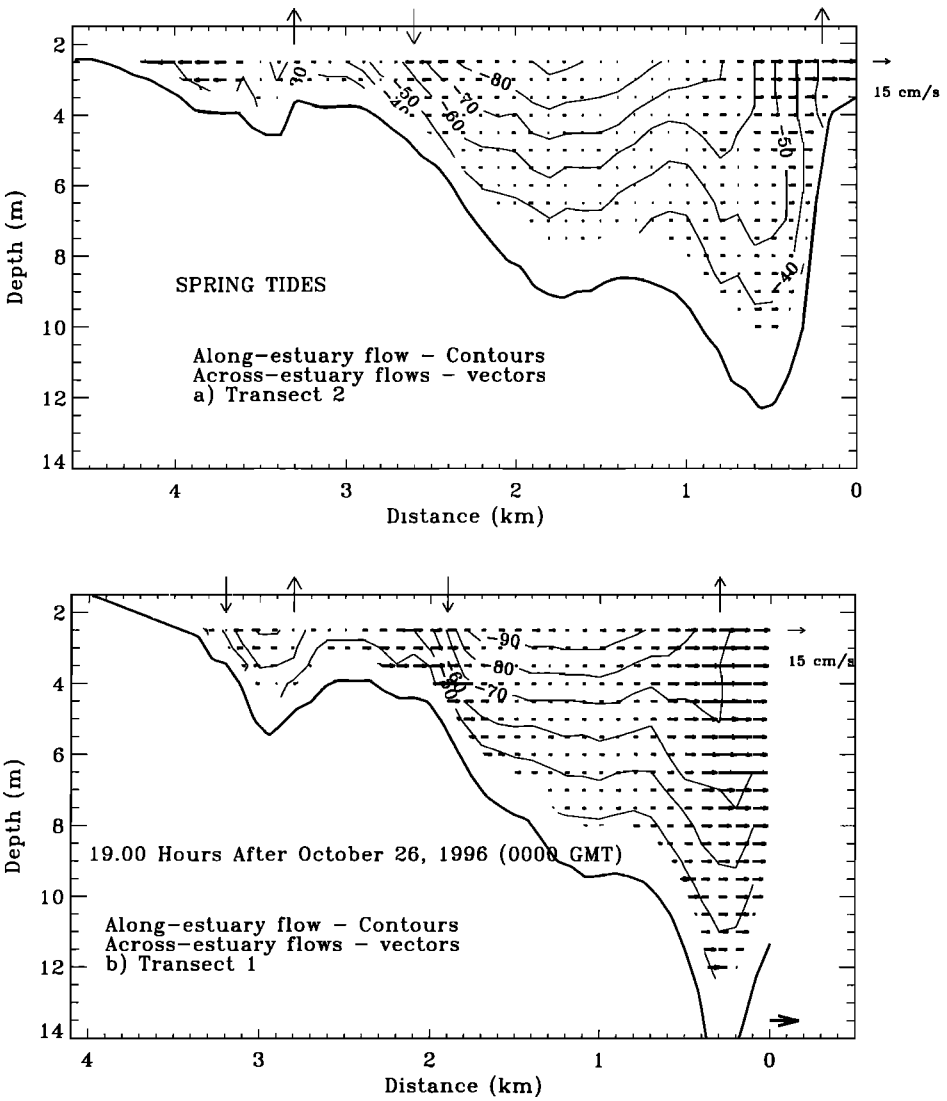

Figure 3. Vertical sections, looking into the estuary, of along-estuary (contours) and across-estuary (vectors) flow (a and b) during ebb and (c and d) during flood of spring tides. These fields were reconstructed with a least squares fit to semidiurnal and diurnal tidal constituents at the times shown. Contour interval is 10 cm s^{-1}. The vertical arrows above 2 m deep indicate convergences (pointing downward) and divergences (pointing upward).

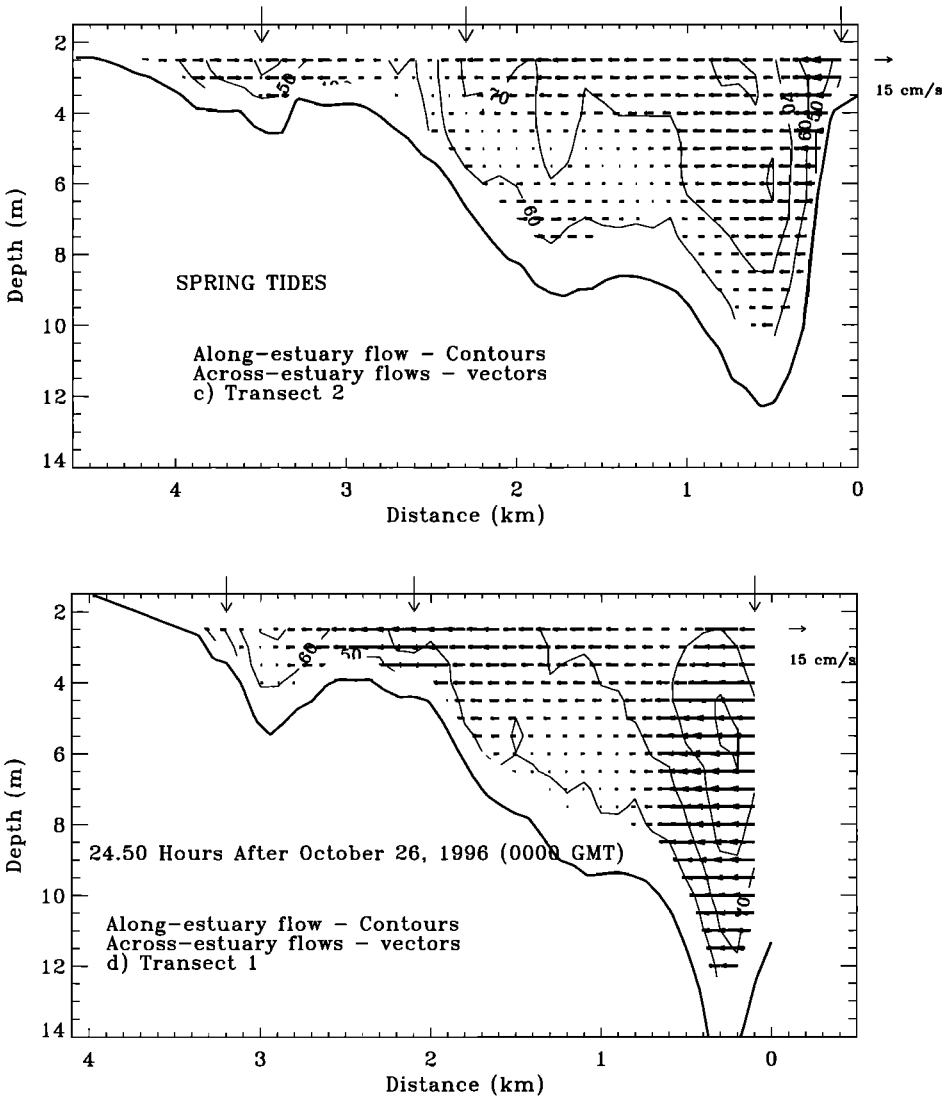

Figure 3. (continued)

discrepancy between transects during ebb flow convergences at the northern edge of the channel (or of the flow core) was due to the geometry of the coastline. In transect 2 the cross-channel ebb flow diverged toward the flanks of the estuary, whereas in transect 1 it converged against the bulkhead of the Newport News Shipyard.

2.2.2. Neap tides. During neap tides, convergences were of the same order of magnitude (10^{-4} s $^{-1}$) but weaker than those during spring tides (Plate 3). As during spring tides, the representation of near-surface divergences with $\partial v/\partial y$ was equivalent to the total horizontal divergence and the divergence of the vertically averaged transverse flow. In contrast to spring tides, there were no regions of persistent convergences through the flood/ebb cycle, although the region over the secondary channel in transect 1 (between 3 and 3.4 km, Plate 3b) exhibited convergences most of the time, markedly during ebb periods. The equivalent region in transect 2 (around 3.5 km, Plate 3a) showed convergences only during flood stages. The behavior over this secondary channel was then very similar from spring to neap tides. Also, similar to spring tides, over the southern edge of the main channel, a surface convergence was observed soon after maximum ebb around 2 km in transect 1 and between 2.5 and 2.8 km in transect 2. An additional consistency with spring tides was the marked convergence during late flood periods over the northern edge of the main channel (between 0 and 0.2 km). As during spring tides, these late flood convergences were more evident in transect 2 than in transect 1. Therefore front formation was expected near the secondary channel and over the northern edge of the main channel at the end of flood and over the southern edge of the main channel after maximum ebb. These were the locations where the convergences ($\partial v/\partial y$) and the bathymetry were coherent in the along-estuary direction. Surface salinity measurements were not available during neap tides, but these front formation patterns were observed as flotsam lines at the times and locations described.

Cross sections of the velocity field showed that the transverse flows associated with flood and ebb convergences were, as in spring tides, mostly in the same direction throughout the water column (Figure 4). Secondary flows expected from curvature effects were not evident either. The near-surface convergences during flood were associated with the edges of the inflow core. Ebb convergences during neap tides developed only over the southern edge of the outflow core. In summary, the most coherent convergences of lateral flow in the along-estuary direction for both spring and neap tides occurred (1) over the northern edge of the main channel

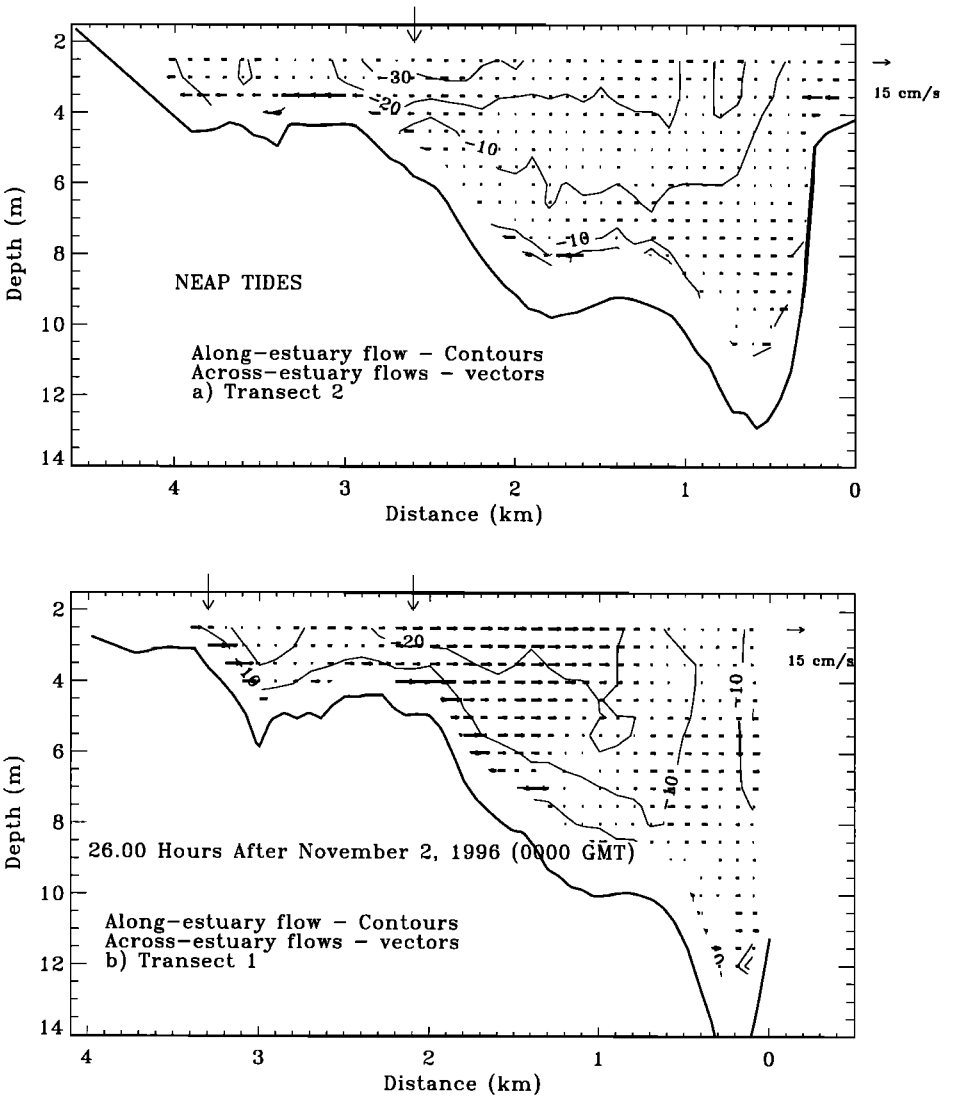

Figure 4. Same as Figure 3, but for neap tides.

during late flood periods and (2) over the southern edge of the main channel after maximum ebb periods. Similar locations and timing of surface convergences have been observed in two Mexican coastal lagoons, Yavaros Bay and Guaymas Bay, where the density gradients are much weaker [*A. Valle-Levinson*, unpublished data, 1999]. This suggested a weak influence of the density gradients on the generation of the convergences. The locations and timing were reproduced reasonably well with a depth-averaged analytic tidal model presented next.

3. Analytic Model

In order to study lateral flow convergences arising from the interaction of tidal flow with bathymetry a model for a semi-enclosed tidal channel with variable lateral depth is presented. The model, fully described by *Li and Valle-Levinson* [1999], is most suitable for narrow estuaries of a few kilometers wide, so that the lateral variation of tidal elevation is small. The model and its solution, which has the character of a progressive wave, are briefly outlined and then applied to a semidiurnal tidal motion over an idealized estuary with prescribed depth functions. The depth functions include the cross-channel depth distributions in the James River where the ADCP observations were obtained. Comparisons of the model results with the observations of tidal convergences are discussed for the most relevant solutions.

3.1. Model Presentation

For simplicity, the model was chosen to have straight parallel side boundaries and a laterally variable depth distribution. The x axis extended along the right boundary (looking into the estuary) and pointed toward the head of the estuary. The y axis extended along the open boundary at x = 0. A single-frequency, semidiurnal tide was imposed at the mouth of the estuary. Both the amplitude and phase of sea level variations at the mouth were assumed uniform across the estuary and were specified. The along-estuary velocity at the head (a solid boundary) vanishes. The depth-averaged, first-order equations for momentum balance and continuity were

$$\frac{\partial u}{\partial t} = -g\frac{\partial \zeta}{\partial x} - \frac{\beta}{h}u \qquad \frac{\partial \zeta}{\partial t} + h\frac{\partial u}{\partial x} + \frac{\partial (hv)}{\partial y} = 0, \qquad (1)$$

where u, v, ζ, h, x, y, t, β, and g were along-estuary velocity (m s^{-1}), lateral velocity (m s^{-1}), elevation (m), water depth (m), along-estuary coordinate (m), lateral coordinate (m), time (s), linearized friction coefficient (m s^{-1}), and the acceleration due to gravity (9.8 m s^{-2}), respectively. The depth function was assumed a function of the cross-estuary direction y only:

$$h=h(y). \tag{2}$$

For a single-frequency cooscillating tide the solution to (1) can be expressed as

$$u=Ue^{i\sigma t} \qquad v=Ve^{i\sigma t} \qquad \zeta=Ae^{i\sigma t}, \tag{3}$$

where σ, i, U, V, and A were the angular frequency of the tide (s^{-1}), the unit imaginary number $\sqrt{-1}$, and the complex amplitudes of the along-estuary velocity (m s^{-1}), lateral velocity (m s^{-1}), and tidal elevation (m), respectively. Substituting (3) into (1) yields:

$$U=-\frac{g}{i\sigma+\beta/h}\frac{\partial A}{\partial x}. \tag{4}$$

For a narrow estuary of a few kilometers wide, it was assumed, on the basis of scaling analysis and numerical model results [*Li*, 1996], that the lateral variations of the tidal elevation and of the along-estuary pressure gradient were much smaller than the corresponding along-estuary variations [*Li and O'Donnell*, 1997; *Li et al.*, 1998]. Therefore, as a first-order approximation, the along-estuary gradient of A in (4) could be treated as independent of y. The validity of this assumption has been supported by an exact solution [*Li and O'Donnell*, 1997] and a perturbation solution [*Li*, 1996] and further discussed by *Li and Valle-Levinson* [1999]. This assumption led to a dramatic simplification of the problem and the solution was given as [*Li and Valle-Levinson*, 1999]

$$A = a\frac{\cos[\omega(x-L)]}{\cos(\omega L)} \tag{5}$$

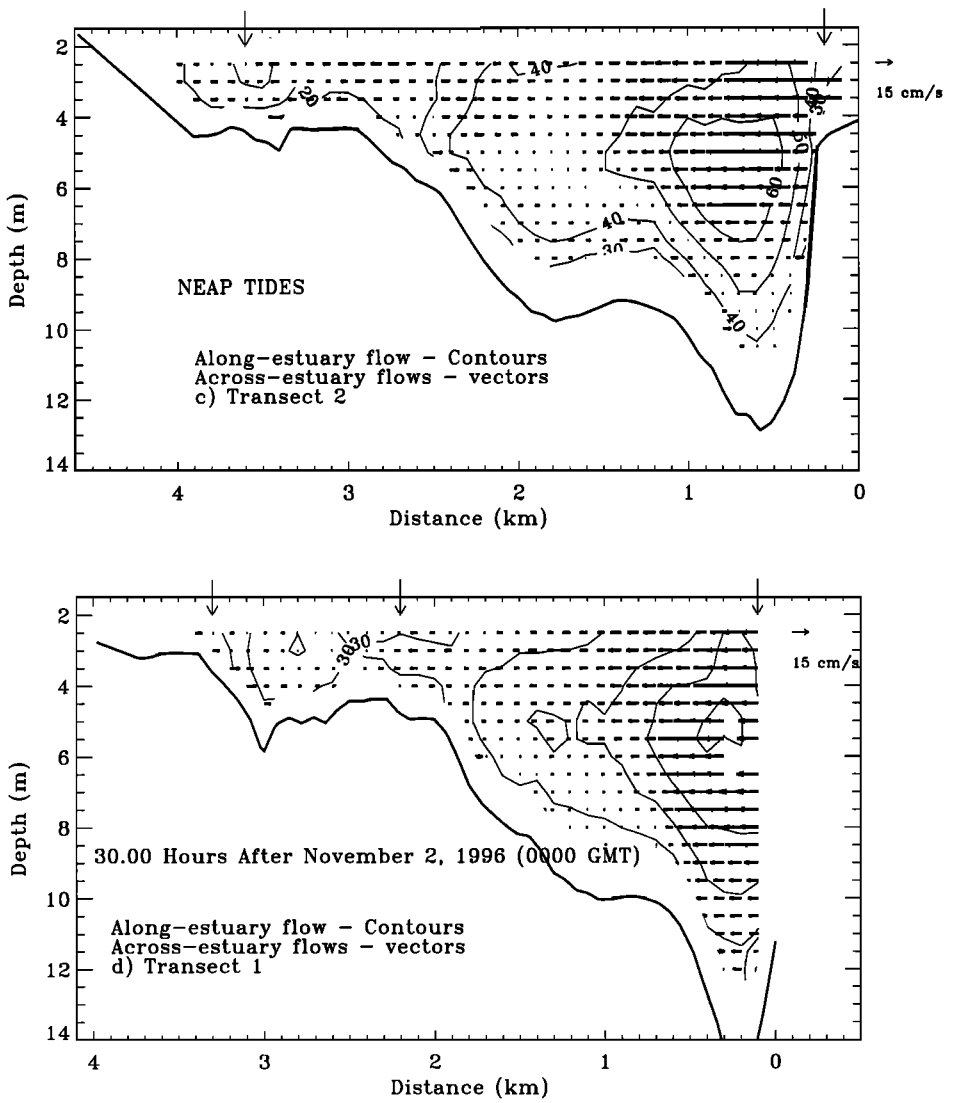

Figure 4. (continued)

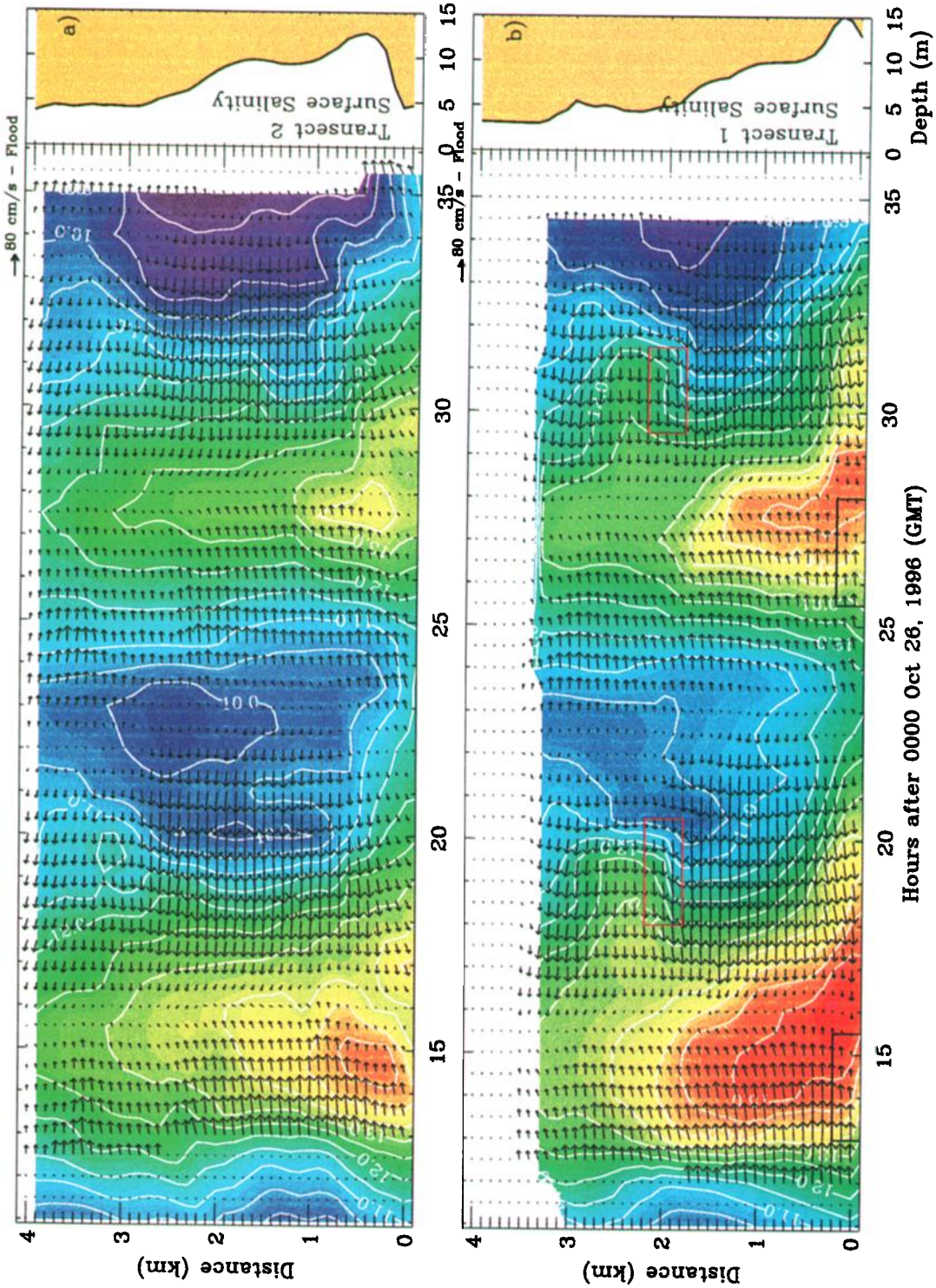

Plate 2. Surface velocity vectors and salinity (colored contours) interpolated to a uniform time-space grid during spring tides. The white contours indicate salinity at intervals of 0.5. The right plots represent the bathymetry of (a) transect 2 and (b) transect 1, with the depth scale appearing on the abscissa. Red rectangles delimit fronts observed during ebb, and blue rectangles indicate fronts observed during flood.

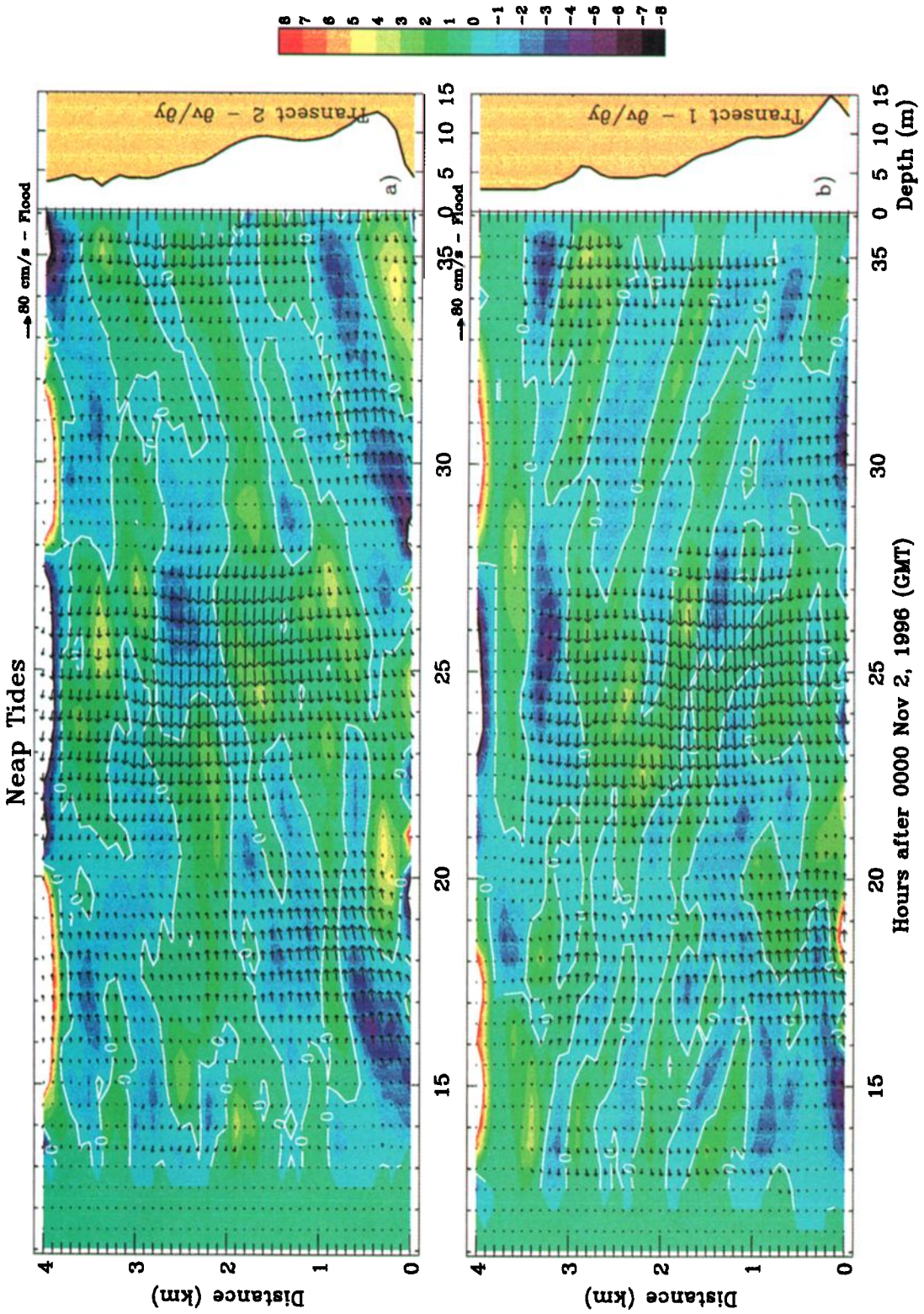

Plate 3. Same as Plate 1, but for neap tides and $\partial v/\partial y$ only.

$$U = \frac{g}{i\sigma + \beta/h} \frac{a\omega}{\cos[\omega(x-L)]} \sin[\omega(x-L)] \quad (6)$$

$$V = -\frac{A}{h}\left(i\sigma y + \int_0^y \frac{gh\omega^2}{i\sigma + \beta/h}\, dy \right) \quad (7)$$

$$\omega^2 = \frac{i\sigma B}{-\int_0^B \frac{gh}{i\sigma + \beta/h}\, dy}. \quad (8)$$

The transverse flow V is insensitive to the transverse momentum balance as it is obtained from the continuity equation (second equation in (1)). The advantage of obtaining V from continuity is that the analytic solution is independent of the transverse momentum balance, which is unknown a priori. The mechanisms that generate convergences can be discerned from the along-estuary dynamics, through continuity, as explained in section 4. By specifying the depth function h, the tidal elevation at the mouth a, the width B and length L of the estuary, the tidal frequency σ, and the friction coefficient β, the solution for the first-order tidal elevation and depth-averaged flow can be calculated from (5) to (7).

3.2. Results With Idealized Depth Distributions

In order to illustrate the interaction of tidal flows and bathymetry and the timing and location of flow convergences the solution (5) to (7) was first applied to several idealized depth distributions. These applications helped to identify distinct patterns of convergence related to bathymetry. The solution was then applied to the depth distributions of transects 1 and 2 in the James River.

The tidal elevation at the mouth, the width of the estuary, and the friction coefficient were prescribed as 0.5 m, 4 km, and 0.0016 m s^{-1}, respectively. The tidal elevation at the mouth (0.5 m) corresponded to the value observed during October 26-27, 1996, at Sewells Point, which is ~12 km seaward from the observation transects. Various values of the length of the estuary (L = 70 to 90 km) were experimented, and the results showed that the maximum amplitude of the along-estuary velocity changed by ~20% for the given range of lengths, while the magnitude of the phase distribution barely changed. The overall distribution of the phase and amplitude of the velocity field across the estuary were consistent for different values of L. The results presented next were for an L of 90 km and at a distance x of 45 km but qualitatively are the same for any distance x. In the following discussions, "left" and "right" directions refer to views into the estuary.

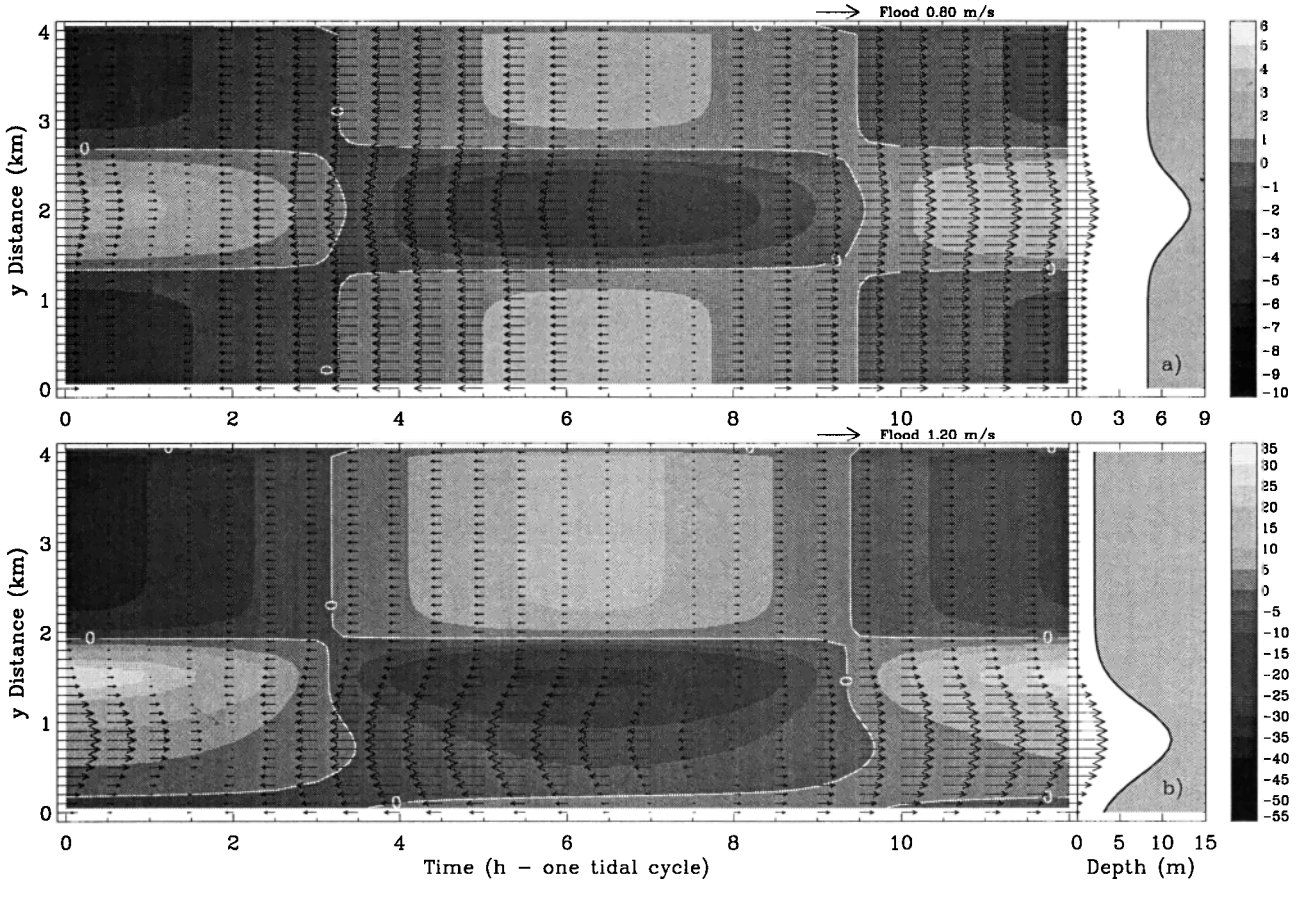

Figure 5. Flow evolution (vectors) and lateral convergences (shaded contours) during one tidal cycle (12 hours only) resulting from the analytic model for idealized bathymetry, cases (a) 1 and (b) 2. The corresponding depth distributions are shown on the right plots with the depth scale appearing on the abscissa. Dark shades denote convergences associated with the palette to the right (10^{-6} s^{-1}). Flood flow points to the right. For Figure 5a, the contour interval is 1×10^{-6} s^{-1}, and the maximum convergence rate is 3×10^{-6} s^{-1}. For Figure 5b, the interval is 5×10^{-6} s^{-1}, with maximum convergence of 3×10^{-5} s^{-1}.

The first case of idealized depth distribution had one channel that was symmetric about the along-estuary axis:

$$h(y) = 5 + 3e^{-(y-B/2)^2/2\times10^5}. \quad (9)$$

This function yielded a maximum depth of 8 m in the middle of the channel and a minimum depth of 5 m over the shoals. The vertically averaged flow field associated with this depth distribution showed well-defined lateral convergences and divergences (Figure 5a). The strongest convergence of 3×10^{-6} s^{-1} developed ~1 hour after maximum ebb in the middle of the channel. During flood periods, convergences appeared over the shoals and divergence in the channel. This pattern resulted from the sense of rotation of the tidal currents. Over the left (looking into the estuary) shoal the flow exhibited counterclockwise rotation, whereas it rotated clockwise over the right shoal. The phase lag between the flow in the channel relative to the shoals was most evident around slack waters and was reflected by along-estuary flow in the channel but cross-estuary flow over the shoals. Hence the phase lag from channel to shoals, together with the sense of rotation of the tidal currents, produced the convergences.

Three variations to the bathymetry depicted in (9) produced revealing results. If the maximum depth in (9) is increased to 11 m (by changing the 3 to a 6), while maintaining 5 m over the shoals, then two convergence regions developed over the edges of the channel, still after maximum ebb currents (not shown). This was produced by increased channel to shoals phase lags; the sense of rotation of the tidal currents was the same as that with the bathymetry of (9). The stronger flow in the middle of the channel effectively separated two convergence regions. Therefore increased steepness of the channel allowed the development of symmetric convergences at either edge of the channel. Another variation of (9) consisted of reducing the bathymetry over the shoals to 1 m with a maximum depth of 4 m (maintaining the 3 in (9)). Symmetric convergences still developed over both edges of the channel but now developed during flood tidal flows (not shown). This was due to reversed rotation patterns of the tidal currents relative to those over the bathymetry of (9), i.e., the currents rotated clockwise over to the left of the channel (looking into the estuary) and counterclockwise over to the right of the channel. This is consistent with *Prandle*'s [1982] idea of frictional effects on the phase, amplitude, and sense of rotation of tidal currents. Decreased steepness in the channel (third variation, changing 3 to 1.5) allowed axial convergence during flood periods, as observed by *Nunes and Simpson* [1985]. Axial convergence is also observed in steady, homogeneous, open channel flow [e.g., *Henderson*, 1966; *Sellin*, 1970].

Another idealized depth distribution had one channel located off the central axis of the estuary:

$$h(y) = 2 + 9e^{-(y-B/5)^2/3\times10^5}. \quad (10)$$

This distribution gave a maximum depth of 11 m at $y = 0.2$ B and a minimum depth of 2 m over an extensive shoal. The strongest convergence of 3×10^{-5} s^{-1} developed again after maximum ebb over the left edge of the channel (Figure 5b). In this case the tidal currents rotated counterclockwise (seen when lateral component is exaggerated) practically everywhere in the domain, as there was no right shoal for clockwise rotation to develop. Therefore, in general, convergence tended to appear toward the left boundary during flood and toward the right boundary during ebb. Owing to the presence of the channel along the right boundary, strong currents in the channel lagged behind the currents over the shoal, and the ebb convergence appeared over the left edge of the channel not against the boundary, as during flood. There was no lateral flow from the right edge of the channel and hence no ebb convergence there. The convergence rates were stronger than in bathymetry (9) owing to greater channel steepness and hence greater phase lags between channel and adjacent shoals. When the same depth shape (10) was moved to the central axis of the estuary, the strongest convergences developed over both edges of the channel (not shown). This was produced by the lateral flows directed from both shoals toward the channel as the tidal flows rotated in opposite directions (clockwise over the right shoal and counterclockwise over the left shoal). These results were relevant to the observations of the James River in the sense that convergence developed over the left edge of the channel (looking into the estuary) after maximum ebb.

Analogous results were obtained with two additional idealized depth distributions represented by

$$h(y) = 2 + 10e^{-(y-B/B_0)^2/Y_d^2} + 3e^{-(y-4B/5)^2/150^2}, \quad (11)$$

where $B_0 = 4$ and 5 and $Y_d = 300$ and 900, respectively, for the two additional depth distributions. These depth distributions showed two channels of different depths as in the James River, although the shape of the deep channel was different for each case. For $Y_d = 300$ and $B_0 = 4$ the convergences after maximum ebb now appeared over the left edge of both channels, consistent with the observations (Figure 6a). The convergence over the deep channel (4×10^{-5} s^{-1}) was greater than that over the shallow channel (1×10^{-5} s^{-1}). In addition, late flood convergences appeared over the right edges of both channels.

The case for which $Y_d = 900$ and $B_0 = 5$ showed a gentler slope in the deep channel, and its deepest point was closer to the right boundary. In this case, the convergence/divergence patterns were the same as in the previous case but now the strongest convergences were associated with the shallow channel (Figure 6b). Therefore the divergences/convergences became weaker in the deep channel as the channel slope decreased (Figure 6). The presence of two channels resulted in ebb to flood convergence patterns that were located between the channels, within 1 km in the lateral direction, i.e., between 2 and 3 km in Figure 6b. The flood/ebb convergence pattern of Figure 6b, between 2 and 3 km, began to show similarities to the pattern observed in the James River as presented next.

3.3. Results With James River Bathymetry

The analytic solution (5) to (7) was applied to the James River estuary with the depth distribution of transects 1 and 2 (Figure 1). Figure 7 shows the evolution of the velocity vectors across the two James River transects during one tidal cycle. The velocity vectors reflected the depth distribution as the strength of the flow was proportional to the local water column depth. Even the secondary channel had a marked influence on the magnitude of the flows. This was the direct effect of bottom friction as indicated by the solution (6). Also, there was a clear phase lag related to bathymetry. The flows over the shallow portions of the estuary turned before the flow in the channel so that the tidal phases occurred earlier to the southwest relative to the northeast. Similarly, the sense of rotation of the tidal currents was counterclockwise over most of the transect. These results were consistent with the distribution of the tidal flows observed across the estuary and in time (Plates 1-3).

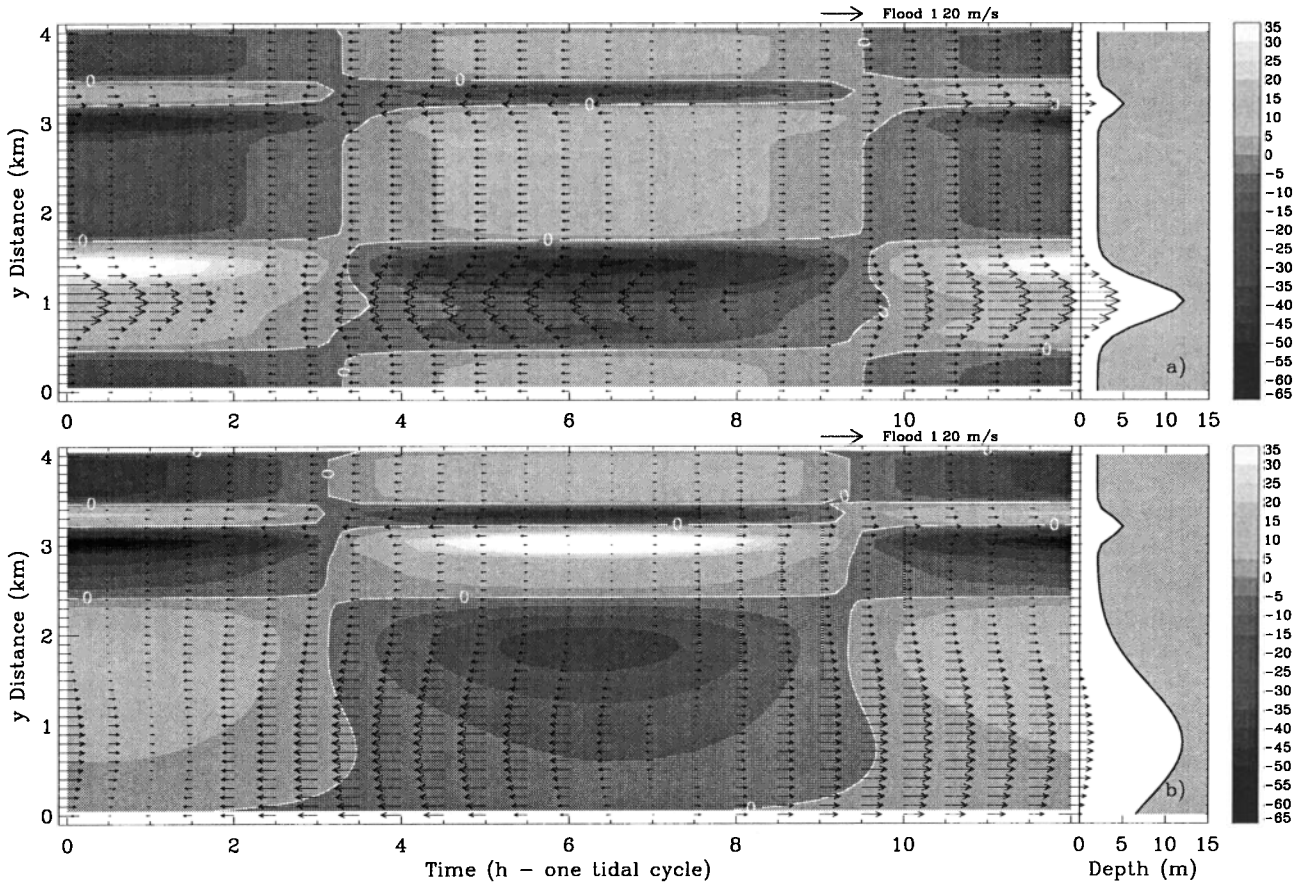

Figure 6. Flow evolution (vectors) and lateral convergences (shaded contours) during one tidal cycle resulting from the analytic model for idealized bathymetry, cases (a) 3 and (b) 4. The corresponding depth distributions are shown on the right plots. Dark shades denote convergences associated with the palette to the right (10^{-6} s^{-1}). Flood flow points to the right. For both plots, the contour interval is 5×10^{-6} s^{-1} and the maximum convergence rates are 4×10^{-5} s^{-1} for Figure 6a and 5×10^{-5} s^{-1} for Figure 6b.

The convergence patterns obtained with the analytic model were qualitatively very similar to those observed (Figure 7). Late ebb convergences were described at around 2 and 3 km for transect 1 and at around 2.5 km for transect 2 in both model and observations. Also, late flood convergences were depicted around 2.5 km for transect 1 and 3.3 km and 0 km for transect 2 in both observations and model. The convergence rates of the model were 5 to 10 times smaller than those observed near the surface but only 2 to 5 times smaller than the convergences calculated with the vertically averaged observed flows. This discrepancy is probably due to the lack of density gradients, which tend to enhance lateral flow [*Dronkers*, 1996] and due to the uniform along-estuary bathymetry in the model. Despite the rough simplifications of the analytic model and the fact that the James River was moderately stratified during the period of observations these results explained the timing and location of the observed convergences of lateral flow as the first-order (as the analytic model) interaction of the tidal flow with the bathymetry.

4. Discussion

The mechanisms that cause convergences of lateral flow along the estuary may be described with the continuity equation (second equation in 1, rewritten):

$$\frac{\partial v}{\partial y} = -\frac{v}{h}\frac{\partial h}{\partial y} - \frac{\partial u}{\partial x} - \frac{1}{h}\frac{\partial \zeta}{\partial t}. \qquad (12)$$

The first term on the right-hand side of (12) is related to the transverse slope of the bathymetry, the second term links the cross-estuary convergences to divergences of along-estuary flow, and the third term depicts the time rate of change of sea surface elevation. By scaling (12) with observations in the James River; $v \sim 0.1$ m s^{-1}, $h \sim 10$ m, $\partial u/\partial x \sim 10^{-5}$ s^{-1}, $\partial h/\partial y \sim 0.05$ to 0.005, and $\partial \zeta/\partial t \sim 4\times10^{-5}$ (m s^{-1}) (1 m in 6 hours), then the bathymetry slope term ranges between 5×10^{-4} and 5×10^{-5} s^{-1}. The along-estuary divergence term is of order 10^{-5}, and the term related to the elevation rate of change is of order 10^{-6}. The term associated with the along-estuary bathymetry gradients $(u/h)\,\partial h/\partial x$ may also be of the same order of magnitude as its transverse counterpart if $u \sim 0.5$ m s^{-1} and $\partial h/\partial x \sim 0.003$. This term is missing from the analytic model (12) but probably influenced the observations. Then, the bathymetry slope and the along-estuary divergence should primarily control the convergence of across-estuary flow.

On the basis of (12) the bathymetry lateral slope should produce convergence of lateral flow (negative $\partial v/\partial y$) over the right edge of the channel (positive slope) with positive v, that is, during flood (Figures 3 and 4). Similarly, convergence will develop over the left edge of the channel (negative slope) when v is negative, i.e., during ebb (Figures 3 and 4). Convergences should be enhanced by divergences of along-estuary flow developing over the right edge of the channel during flood and over the left edge of the channel during ebb. Such divergences should be proportional to the tidal

forcing, being greater during spring tides than during neap tides. The convergences toward the channel would tend to add mass there and would therefore tend to increase the magnitude of the along-estuary flow in the channel. These kinematic explanations correspond to the patterns of convergence observed.

An additional explanation of the convergence patterns may be drawn from the solution for the lateral velocity. According to (7), V is a function of y multiplied by the tidal elevation A (which is nearly independent of y). Thus the phase of V is a function of y plus the phase of A. The phase difference between V and A is then only a function of y, i.e., the cophase lines for V are parallel to the lateral boundaries. This means that for a bathymetry mostly changing across the channel a lateral convergence or divergence tends to happen along the channel at certain phase of A. This is why the observed lines of convergence develop along the channel at certain tidal phases. Furthermore, friction causes the tidal flow in the channel to lag that on the shoals. In the James River this phase lag can be up to 1 hour. This means that during flood, while the shallow water has reached its maximum strength of inward flow, the adjacent deep water has not. This will cause a flood convergence over the slope of the right channel (looking into the estuary) as shown in Figure 8, given a counterclockwise rotation of the tidal ellipses as observed in the James. Similarly during ebb, the shoal on the left side reaches the maximum strength of outward flow, while the deep water is lagging, which causes an ebb convergence over the left slope (Figure 8). The sense of rotation of the tidal ellipse depends on the phase difference between V and U. When the phase difference is <180°, the rotation is clockwise. Otherwise, it is counterclockwise.

To study along-estuary front dynamics in estuaries, most studies have pointed to the steady state lateral balance between the baroclinic pressure gradient and friction [e.g., *Nunes and Simpson*, 1985; *Swift et al.*, 1996]. Recently, the Coriolis acceleration [*C.T. Friedrichs and A. Valle-Levinson*, manuscript in preparation, 2000] and the nonlinear effects [*Valle-Levinson and Atkinson*, 1999] have been shown to be relevant to this balance in areas of sharp bathymetry. The present study shows that bottom friction is important in the evolution of convergences, which typically lasted between 1 and 2 hours. In addition, there are four mechanisms linked to the transverse variability of along-estuary properties not included in the analytic model presented here that should contribute to the magnitude of the convergences. The first is associated with the transverse shears of the along-estuary flow through nonlinear advection [*A. Valle-Levinson et al.*, On the linkage among density, flow, and bathymetry gradients at the entrance to the Chesapeake Bay, submitted to Journal of Geophysical Research, 2000). The second is related to the transverse variability of the along-estuary baroclinic pressure gradient, similar to the mechanism proposed by *Nunes and Simpson* [1985]. In the study area the transverse density gradients play an important dynamic role [*Valle-Levinson et al.*, 2000] and should enhance the convergence rates while maintaining the stability of the fronts, which are influenced by strong transverse shears. The

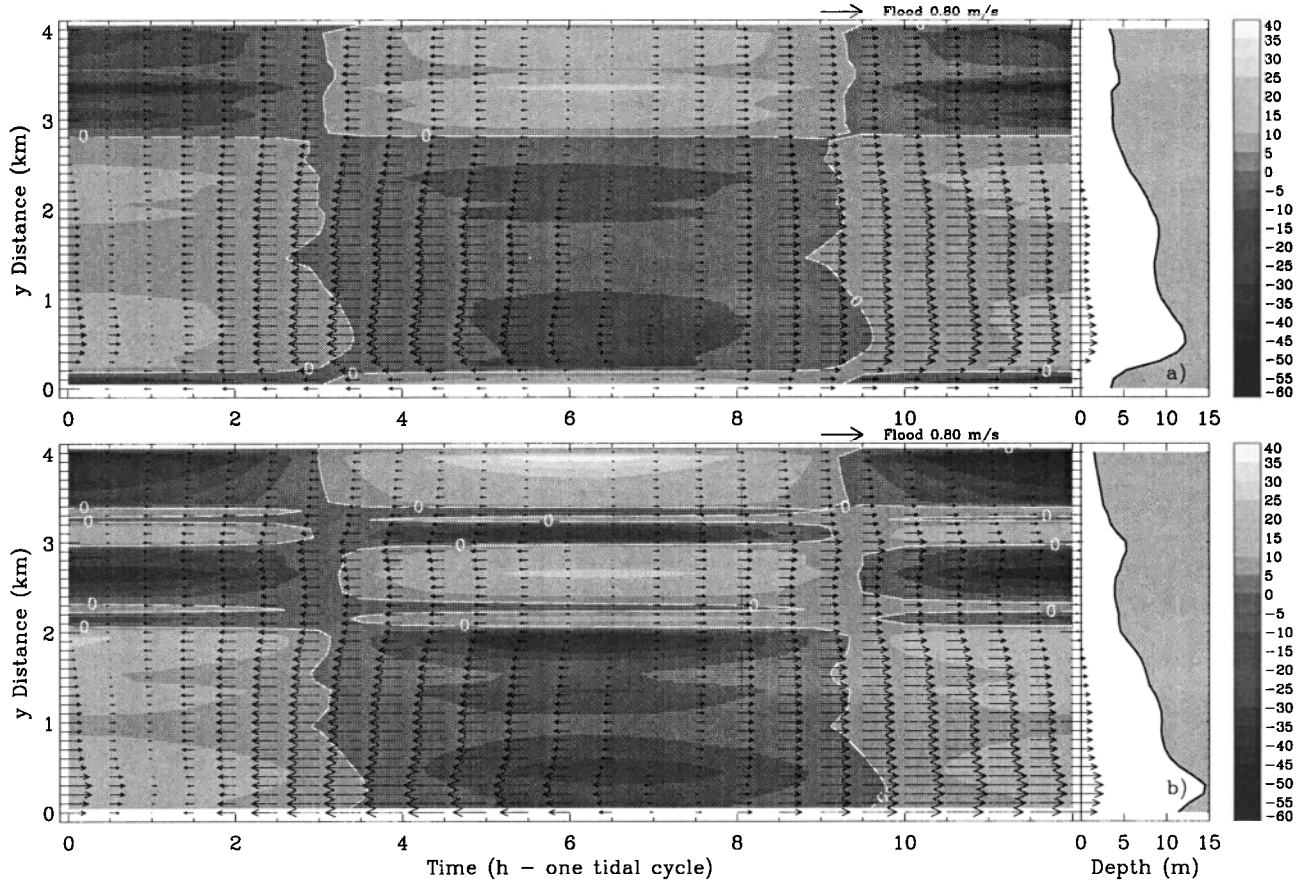

Figure 7. Same as in Figures 5 and 6 but for the James River bathymetry at transects (a) 2 and (b) 1. For both plots, the contour interval is 5×10^{-6} s^{-1}, and the maximum convergence rates are 2×10^{-5} s^{-1} for Figure 7a and 3×10^{-5} s^{-1} for Figure 7b.

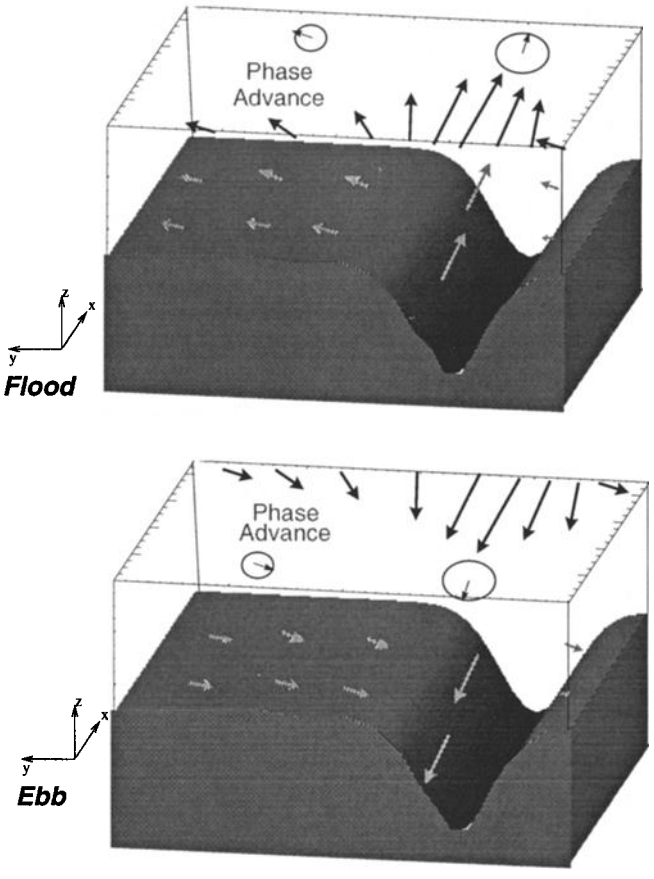

Figure 8. Schematic of the mechanisms generating convergences. The same mechanism applies for flood and ebb periods. For flood the diagram is looking into the estuary. For ebb the diagram is looking toward the mouth of the estuary. The ellipticity of the tidal ellipses is greatly exaggerated to illustrate the transverse flows.

third mechanism is linked to the transverse variations in vertical mixing [*Bowman and Iverson*, 1977], which requires elucidation of the vertical structure of the flow and density fields. The fourth arises from the along-estuary bathymetry gradients $(u/h)\ \partial h/\partial x$, which may be of the same order of magnitude as the dominant terms in (12). Therefore future studies should take into account the influence and evolution of the above forcing mechanisms throughout the tidal cycle. The mechanisms proposed here account for ~20-50% of the magnitude of the convergences produced by the vertically averaged flow observed and explain the timing and location of such convergences.

5. Conclusions

Observations of convergence of lateral flow ($\partial v/\partial y$) at two transects across the James River estuary showed consistent patterns from spring to neap tidal currents. The strength of the convergences was proportional to the slope of the channel bathymetry and to the tidal forcing. The convergences were produced by the phase lag between channel and shoals, which produced flows rotating toward the channel from the shoals. Convergences after maximum ebb developed over the left (looking into the estuary) edge of the channel at both transects. Late flood convergences occurred over the right edge of the channel at both transects. In the portion of the James River studied the right edge of the shallow channel and the left edge of the deep channel were within 1 km. Therefore that region between the two edges exhibited convergences during both flood and ebb periods. The persistence of the convergences along the estuary appeared to be related to the along-estuary coherence scale of the bathymetry. Results from a depth-averaged tidal model confirmed these convergence patterns and indicated that the first-order interaction of the tidal current with the bathymetry was responsible for the location and timing of the convergences. Model results also showed that axial convergences during flood stages, as observed in other studies [e.g., *Nunes and Simpson*, 1985], developed from the interaction of tidal currents with bathymetry over a shallow estuary with gentle channel slope. Consequently, the density field played a minor role in causing convergences of lateral flow along the estuary. The observations suggested that the density field, through its interaction with the tidal flow and the bathymetry, reinforced the magnitude of the convergences and formed along-estuary fronts over the edge of the channels.

Acknowledgments. This project was funded by the U.S. National Science Foundation under project OCE-9529806 to A.V.L., OCE-9530395 to K.C.W., and OCE-9530394 to K.M.M.L. C.L. was supported by the Center for Coastal Physical Oceanography. Dozens of faculty members, staff, and students from Old Dominion University, University of Delaware, and State University of New York at Stony Brook participated in the field work, and their help was invaluable. Thanks to R. Bray, R.C. Kidd, and W. Check for field assistance. More information about this project may be found at http://www.ccpo.odu.edu/~arnoldo/transcope/ transcope.html

References

Bowman, M.J., and R.L. Iverson, Estuarine and plume fronts, in *Oceanic Fronts in Coastal Processes*, pp. 87-104, Springer-Verlag, New York, 1977.

Brown, J., W.R. Turrell, and J.H. Simpson, Aerial surveys of axial convergent fronts in UK estuaries and the implications for pollution, *Mar. Pollut. Bull., 22*(8), 397-400, 1991.

Chant, R.J., and R.E. Wilson, Secondary circulation in a highly stratified estuary, *J. Geophys Res., 102*, 23,207-23,215, 1997.

Dronkers, J., The influence of buoyancy on transverse circulation and on estuarine dynamics, *Buoyancy Effects on Coastal and Estuarine Dynamics, Coastal Estuarine Stud.*, vol. 53, edited by David G. Aubrey and Carl T. Friedrichs, pp. 341-356, AGU, Washington, D. C., 1996.

Ferrier, G., and J.M. Anderson, A multi-disciplinary study of frontal systems in the Tay Estuary, Scotland, *Estuarine Coastal Shelf Sci., 45*, 317-336, 1997..

Geyer, W.R., Three-dimensional tidal flow around headlands, *J. Geophys. Res., 98*, 955-966, 1993.

Henderson, F.M., *Open Channel Flow*, 522 pp., Macmillan, Indianapolis, Indiana, 1966.

Huzzey, L.M., and J.M. Brubaker, The formation of longitudinal fronts in a coastal plain estuary, *J. Geophys. Res., 93*, 1329-1334, 1988.

Joyce, T. M., On in situ calibration of shipboard ADCPs, *J. Atmos. Oceanic Technol., 6*(1), 169-172, 1989.

Li, C., Tidally induced residual circulation in estuaries with cross channel bathymetry, Ph.D. dissertation, 242 pp., Univ. of Conn., Storrs, 1996.

Li, C., and J. O'Donnell, Tidally driven residual circulation in shallow estuaries with lateral depth variation, *J. Geophys. Res., 102*, 27,915-27,929, 1997.

Li, C., and A. Valle-Levinson, A two-dimensional analytic tidal model for a narrow estuary of arbitrary lateral depth variation: The intra-tidal motion, *J. Geophys. Res., 104*, 23,525-23,543, 1999.

Li, C., J. O'Donnell, A. Valle-Levinson, H. Li, K.-C. Wong,

K.M.M. Lwiza, Tide induced mass-flux in shallow estuaries, in *Ocean Waves Measurement and Analysis*, vol. 2, edited by B. L. Edge and J. M. Hemsley, pp. 1510-1524, Am. Soc. Civ. Eng., Reston, Va., 1998.

Nunes, R.A., and J.H. Simpson, Axial convergence in a well-mixed estuary, *Estuarine Coastal Shelf Sci., 20,* 637-649, 1985.

Prandle, D., The vertical structure of tidal currents, *Geophys. Astrophys. Fluid Dyn., 22,* 29-49, 1982.

Sarabun, C.C., Structure and formation of Delaware Bay fronts, Ph.D. dissertation, 229 pp., Univ. of Delaware, Newark, 1980.

Sellin, R.H.J., *Flow in Channels,* 149 pp., Gordon and Breach, Newark, N.J., 1970.

Simpson, J.H., and W.R. Turrell, Convergent fronts in the circulation of tidal estuaries, in *Estuarine Variability*, edited by D.A. Wolfe, pp. 139-152, Academic, San Diego, Calif., 1986.

Sletten, M.A., G.O. Marmorino, T.F. Donato, D.J. McLaughlin, and E. Twarog, An airborne, real aperture radar study of the Chesapeake Bay outflow plume, *J. Geophys. Res., 104,* 1211-1222, 1999.

Swift, M.R., D.W. Fredriksson, and B. Celikkol, Structure of an axial convergence zone from acoustic Doppler current profiler measurements. *Estuarine Coastal Shelf Sci., 43,* 109-122, 1996.

Turrell, W.R., J. Brown, and J.H. Simpson, Salt intrusion and secondary flow in a shallow, well-mixed estuary, *Estuarine Coastal Shelf Sci., 42,* 153-169, 1996.

Valle-Levinson, A., and L.P. Atkinson, Spatial gradients in the flow over an estuarine channel, *Estuaries*, 22(2A), 179-193, 1999.

Valle-Levinson, A., and J. O'Donnell, Tidal interaction with buoyancy driven flow in a coastal plain estuary, in *Buoyancy Effects on Coastal and Estuarine Dynamics, Coastal Estuarine Stud.*, vol. 53, edited by David G. Aubrey and Carl T. Friedrichs, pp. 265-281, AGU, Washington, D. C., 1996.

Valle-Levinson, A., K.C. Wong, and K.M.M. Lwiza, Fortnightly variability in the transverse dynamics of a coastal plain estuary, *J. Geophys. Res., 105*, 3413-3424, 2000.

C. Li and A. Valle-Levinson, Center for Coastal Physical Oceanography, Department of Ocean, Earth, and Atmospheric Sciences, Old Dominion University, Norfolk, VA 23529. (arnoldo@ccpo.odu.edu)

K.M.M. Lwiza, Marine Sciences Research Center, State Univerisiy of New York, Stony Brook, NY 11794.

K.-C. Wong, College of Marine Studies, University of Delaware, Newark, DE 19716.

(Received April 2, 1999; revised December 10, 1999; accepted January 4, 2000.)